Symmetric splitting for the system $^{32}S + ^{238}U$ at energies near and below the barrier

R. Freifelder,* P. Braun-Munzinger, P. DeYoung,† R. Schicker, S. Sen, and J. Stachel
Department of Physics, State University of New York at Stony Brook, Stony Brook, New York 11794
(Received 23 May 1986; revised manuscript received 10 February 1987)

The total capture cross section for the system $^{32}S + ^{238}U$ has been measured at energies from 0.93 to 1.08 times the *s*-wave interaction barrier by detecting coincident fission fragments following full momentum transfer reactions. The subbarrier cross section cannot be reproduced by a one-dimensional barrier penetration model. Using a quantum mechanical coupled channels model, good agreement is obtained. The measured angular distributions of fission fragments were compared to the predictions of saddle and scission point transition state theory. Saddle point transition state model calculations fail to reproduce the data, while scission point transition state calculations are in agreement with their qualitative trend. Evidence for nonequilibrium processes is presented.

I. INTRODUCTION

The fusion of two nuclei into a completely equilibrated system at energies below the top of the interaction barrier is a well known example of quantum mechanical tunneling. Much information about the height and width of the barrier for a large number of systems has been obtained by measuring this fusion probability as a function of the center of mass energy.[1,2] For light systems, typically, the evaporation residues are measured, while for heavier systems the fission cross section must, in addition, be measured. The fission process is interesting in its own right, e.g., the question of the applicability of transition state theory to describe fission of very heavy systems has been actively debated.[3–6]

In light systems the term fusion describes a well defined reaction in which a compound nucleus is formed. For heavy systems a more general term, capture,[7,8] has been used to describe reactions in which there is a large mass asymmetry in the entrance channel and a symmetric or nearly symmetric mass splitting in the exit channel. In our discussion below we will use the more general term, capture, in this regard without making a distinction as to whether the system has crossed over the conditional saddle point or not. The experiments reported here aim at exploring symmetric splitting reactions near and below the barrier for the very heavy system $^{32}S+^{238}U$ which has a total charge $Z=108$ and total mass $A=270$ corresponding to $Z^2/A=43.2$. This system is also of interest since it is at the boundary of where the extra push formalism might become relevant.[7] It has an effective entrance channel fissility, $X_e=(Z^2/A)_{\rm eff}/(Z^2/A)_{\rm crit}$ of 0.68 with $(Z^2/A)_{\rm eff}=31.9$ and $(Z^2/A)_{\rm crit}=47.25$. According to extra push systematics an extra push energy is necessary when X_e exceeds 0.70 ± 0.01.

The experiments spanned an energy range from approximately 11 MeV below the interaction barrier to 13 MeV above it. Similar experiments using reversed kinematics have been performed elsewhere at both these and higher energies.[8] In this paper we will focus on the lower energy range and show that a measurable capture cross section exists even when the bombarding energy is below the pocket in the potential predicted by a simple one-dimensional model. The capture data will be compared to a quantum mechanical coupled channels calculation. The results of the calculations show that by including only the ground state and the first excited state in ^{238}U the total capture data can be well reproduced.

Systematics show that for this system the evaporation residue cross section is expected to be very small[9] and hence the capture cross section can be measured by detecting fission fragments in the exit channel. Therefore, measurements of the angular distribution of fission fragments were made over a large angular range. This provided the possibility of studying the fission decay from a very heavy ($A=270$) system. One theory describing such decay is the saddle point transition state theory.[10,11] In some systems the predictions based on this theory were unable to account for the observed fission fragment angular distributions.[3,12] For very heavy systems the saddle point shape is very different from the scission point shape and results using the scission point as the transition state for calculating the angular distribution of fission fragments will be described.

To search for possible nonequilibrium effects in this reaction the masses of the fission fragments were measured as a function of the scattering angle. The use of a saddle point transition state theory to describe the angular distribution of fission fragments would be called into question by the presence of mass asymmetric splitting. However, the use of a scission point transition state theory may still be valid as that theory merely assumes the existence of an equilibrated system outside of the saddle point and does not assume compound nucleus formation.

In Sec. II we describe the experimental aspects of the measurements and in Sec. III the results. In Sec. IV the capture data will be compared to the predictions of one-dimensional and multi-dimensional barrier penetration calculations. The angular distributions will be discussed in Sec. V and compared to predictions of the saddle point and scission point transition state models.

II. EXPERIMENTAL METHOD

The experiments were performed using ^{32}S beams from the Stony Brook Tandem-Superconducting Linac Ac-

celerator. The beam irradiated targets of ^{nat}U of areal density 200 $\mu g/cm^2$ which were backed by either a 200 $\mu g/cm^2$ ^{nat}Ni foil or a 50 $\mu g/cm^2$ ^{nat}Al foil and were kept at a potential of $+22$ kV to prevent electrons from hitting the detectors. Laboratory energies of 171.0, 179.0, 188.0, and 199.0 MeV were used corresponding to center of mass energies 150.7, 157.8, 165.7, and 175.4 MeV as compared to an s-wave interaction barrier of approximately 161.8 MeV (using the potential of Ref. 13). The capture cross section was measured by detecting coincident fission fragments from the reaction. Fission fragments as well as elastically and inelastically scattered particles were detected in two position sensitive parallel plate avalanche counters which provided time of flight and position information.

A small circular counter (5 cm in diameter) which was position sensitive with respect to the scattering angle θ was located at backward angles ($72° \leq \theta_{lab} \leq 154°$). It was placed 10 cm from the target and covered an angular range of $\pm 12.4°$, with a resolution of $\Delta\theta \approx 0.4°$. Its out of plane acceptance angle was approximately $\pm 6°$. A large rectangular detector (20×15 cm^2) was located at forward angles ($13.8° \leq \theta_{lab} \leq 72°$) 40 cm from the target. This detector was position sensitive both in θ and the polar angle ϕ, covering an angular range in θ of $\pm 14.3°$ and in ϕ of $\pm 10.8°$. Its angular resolution was $\Delta\theta = \Delta\phi = 0.1°$.

The relative angle between the two detectors was chosen to detect in coincidence fission fragments following full momentum transfer. The two detectors were moved so as to cover the range $90° \leq \theta_{c.m.} \leq 166°$ at $E_{lab} = 179.0$, 188.0, and 199.0 MeV and $127° \leq \theta_{c.m.} \leq 169°$ at $E_{lab} = 171.0$ MeV. The beam current was monitored in a Faraday cup and in two solid state monitor detectors which were placed out of plane at scattering angles of $\approx 25°$ on either side of the beam.

Time of flight information was used to discriminate between elastic (and quasi-elastic) processes and fission events. The time resolution of the avalanche counters was measured to be ≤ 300 ps and the intrinsic time resolution of the pulsed beam (which had a repetition rate of 106.6 ns) was between 350 ps and 1 ns. In addition to time of flight and position information, a ΔE signal from each detector was recorded. Figure 1 shows a typical two dimensional plot of the relative time of flight between two coincident particles hitting the detectors and the ΔE signal from the larger counter.

Because particles were measured in coincidence, the only type of elastic or quasi-elastic event that could be detected was a ^{32}S scattered into backward angles and a ^{238}U scattered forward. These events are indicated in the figure. The large central region corresponds primarily to fission fragments following a collision in which most of the momentum of the incoming ^{32}S was transferred to the combined system. The amount of momentum transferred was measured to be $\geq 95\%$, assuming Viola systematics.[14]

The events on the right-hand side of Fig. 1 correspond to reactions where a quasi-elastic ^{32}S was detected in the large detector in coincidence with a fission fragment. Figure 1 shows that, based on the relative time of flight, discrimination between the elastic or quasi-elastic events and fission events was easily achieved. To suppress additional background due to sequential fission of the ^{238}U fission, fragments were first selected according to Fig. 1. Angular correlation spectra were then obtained and a typical example is shown in Fig. 2. These spectra exhibited clear, correlated peaks corresponding to kinematically allowed coincident fission fragments following full momen-

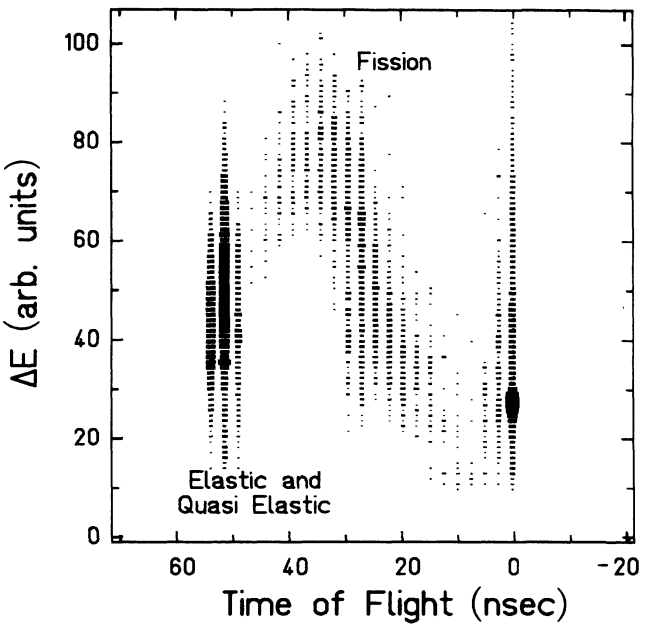

FIG. 1. Two dimensional plot of the relative time of flight of the two particles detected vs the energy loss ΔE in the large detector at $E_{c.m.} = 165.7$ MeV.

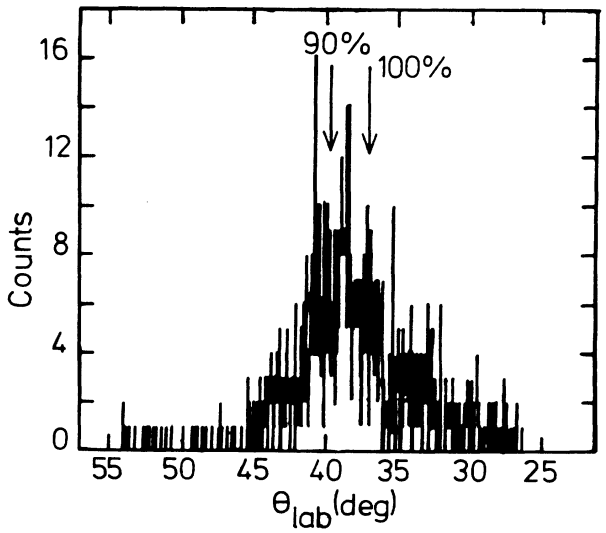

FIG. 2. Position spectrum, at $E_{c.m.} = 165.7$ MeV, of fission fragments in the large detector correlated with events occurring within a small angle slice ($\approx 5°$) in the small detector, plotted as a function of the laboratory detection angle. The arrows indicate the expected position for 90% and 100% momentum transfer.

tum transfer (see figure). The flat distribution, in addition to the peak, displays background due to sequential fission in which one of the fission fragments from the ^{238}U is not detected. These events could be subtracted quantitatively. Sequential fission in which both fragments from the ^{238}U are detected following inelastic scattering into the grazing angle lead to fold angles of $\approx 130°$ or smaller in the energy range considered. Therefore these would be well separated from the full momentum transfer peak (with a fold angle of $\approx 152°$) in Fig. 2 and do not contribute any background.

The differential cross section in the laboratory frame was then calculated by taking into account the appropriate solid angles in the small backdetector and normalizing the yield to the Rutherford scattering measured by the two monitor detectors.

For the measurements at $E_{c.m.} = 157.8$ and 165.7 MeV the mass of the fission fragments was also determined. For a true compound nucleus reaction the mean value of this distribution is expected to be centered about $A_{CN}/2 = 135$ and should be independent of the center of mass scattering angle. Deviations from this behavior have been observed[8,15] and could be taken as signatures that the reaction is taking place on a timescale that is faster than the time for equilibration in the mass degree of freedom. Fragment masses were determined by using the measured velocity vectors of the fission fragments and assuming two body kinematics. Calibration was provided by elastic scattering. Selecting only fission fragments following full momentum transfer yields typical mass spectra as shown in Fig. 3.

No corrections for light particle emission were made. Since the angular distribution of neutrons emitted from the primary fragments is assumed to be isotropic in the reference frame of the fragment, the measured velocity vector is averaged over all neutron emission angles and represents the average kinetic energy of the primary fragment. Therefore the average kinetic energy and mass of the fission fragments prior to neutron evaporation was calculated.[16–18]

The intrinsic mass resolution was calculated using a Monte Carlo simulation to include the effects due to the finite position and time resolution of the detectors and the beam. These calculations indicate that for the masses and angles covered the mass resolution was $\approx 10\%$.

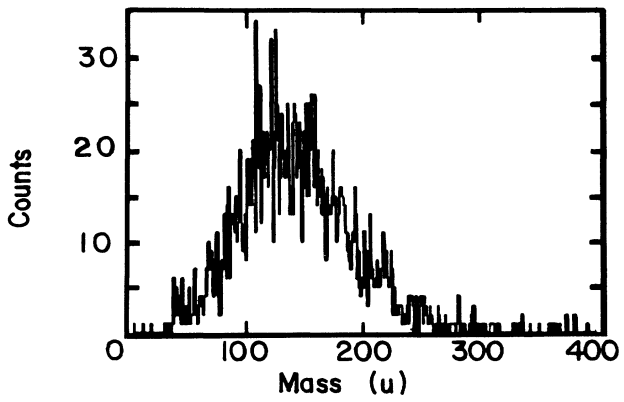

FIG. 3. Typical mass spectrum at $E_{c.m.} = 157.8$ MeV.

III. EXPERIMENTAL RESULTS

In Fig. 4 the measured differential cross sections are shown. The errors shown are statistical uncertainties; for cases where several measurements are available, the weighted average is shown and the errors are propagated accordingly. The data show variations beyond purely statistical errors and display systematic uncertainties. Four sources of errors were considered: (1) Inaccuracies due to background subtraction; these were estimated to be small ($<2\%$) for the three highest energies where the amount subtracted varied between 10% and 15%. For the lowest energy the amount subtracted approached 50% and here an uncertainty of $\approx 9\%$ was estimated by fitting various order polynomials ($N=0$–3) to the background. (2) Errors due to inaccuracies in the solid angle determinations ($\approx 8\%$). (3) Errors due to detector efficiency are negligible; the efficiency was measured to be $>98\%$. (4) Normalization errors due to inaccuracies in the absolute angles and positions of the monitor detectors ($\approx 20\%$). Errors (2) and (3) affect the overall integrated cross section only, whereas (1) and (4) account for the fluctuations in

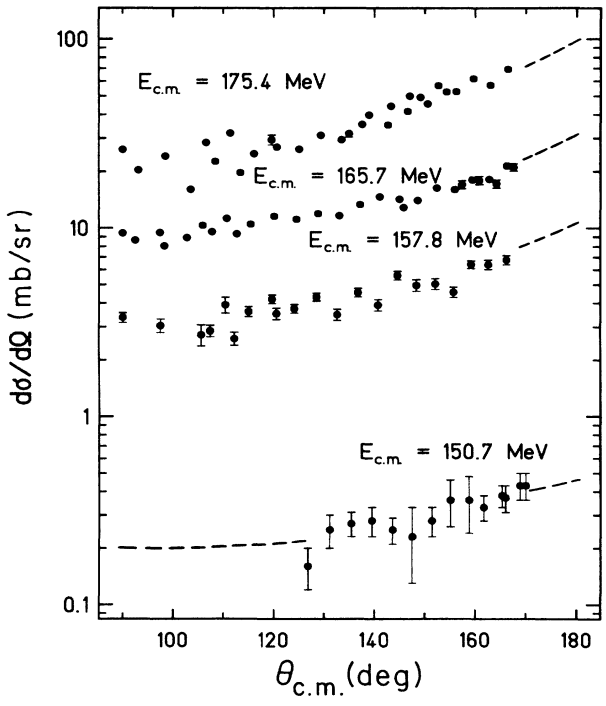

FIG. 4. Angular distributions of fission fragments at $E_{c.m.} = 150.7$, 157.8, 165.7, and 175.4 MeV. Only statistical errors are shown. The size of the systematic error in the data can be judged from the fluctuations of the data points and is discussed in the text. The dashed lines indicate extrapolations used to determine the integrated cross sections (see text).

the differential cross section.

The capture cross section was obtained by integrating the angular distributions. Since the experimental data only covered angles $\theta_{c.m.} \leq 170°$, the points for angles $170° \leq \theta_{c.m.} \leq 180°$ were smoothly extrapolated (dashed lines in Fig. 4). The uncertainty induced by this extrapolation is given in Table I along with the capture cross sections and their statistical and systematic errors.

At $E_{c.m.} = 157.8$ and 165.7 MeV the masses of the fission fragments were determined for $127° \leq \theta_{c.m.} \leq 170°$. The center of mass scattering angle was calculated by assuming symmetric fragmentation. Assuming asymmetric fragmentation with a mass ratio of 2:1 shifts the average center of mass scattering angle by $\leq 1.5\%$. The variation in the Jacobian as a function of mass asymmetry was then taken into account and the centroids of the mass distribution were calculated by fitting a Gaussian to the data. The Jacobian shifts the centroid toward heavier masses in the center of mass system and this shift amounts to $\leq 10\%$. The centroids from different angle settings of the detector (which allowed for overlapping measurements to be made) were well within the errors. The results are shown in Fig. 5. At both energies one observes a correlation between the mass of the fragment and the center of mass scattering angle. This may be taken as evidence for nonequilibrium effects in the present reaction.

IV. COMPARISON OF THE DATA WITH CAPTURE CALCULATIONS

By studying the fusion cross section, information on the shape of the effective ion-ion potential can be obtained. However, static or dynamic deformations have to be taken into account in a description of the reaction as they could significantly modify the effective ion-ion potential. Different nuclear shapes or orientations that have their surfaces closer to each other for a given center of mass distance will lower the interaction barrier. Hence the probability for tunneling through this lower interaction barrier will increase. Models which take into account static deformations,[2] zero point motion,[19,20] neck formation,[2,21] or other mechanisms[22] have predicted larger total fusion cross sections than one-dimensional calculations employing static spherical potentials.

Recently,[20,23–27] much effort has been devoted to incorporating several of the above mentioned effects without *ad hoc* assumptions by explicitly taking into account the coupling to low lying excited states in the target and/or the projectile in calculating the fusion cross section σ_{fus}. The argument is based on unitarity of the S matrix, i.e.,

$$1 = \sum_{\beta} |S^{\alpha,\beta}|^2 , \tag{1}$$

where β sums over all available channels. For a system without strong transfer or deep inelastic reactions the S matrix can be though of as being comprised of only elastic, inelastic, and capture channels. Then one can determine the capture cross section, σ_{capt}, independent of whether or not compound nucleus formation takes place by calculating the coherent part of the reaction, i.e., the elastic and inelastic channels. Thus, σ_{capt} is determined

TABLE I. Experimentally determined capture cross sections for $^{32}S + ^{238}U$ including statistical and systematical errors and errors due to the extrapolation of the data to 180°.

$E_{c.m.}$ (MeV)	E_{lab} (MeV)	σ_{capt}^{expt} (mb)	Statistical and systematic error (mb)	Extrapolation error (mb)
150.7	171.0	3.3	0.8	0.4
157.8	179.0	51	11	1
165.7	188.0	151	33	4
175.4	199.0	429	94	8

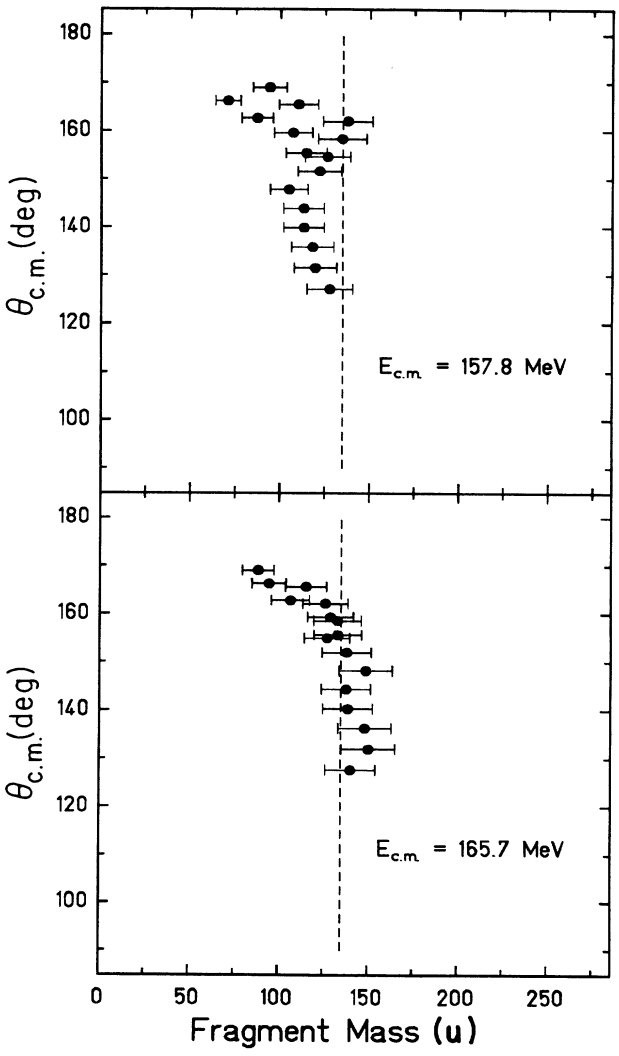

FIG. 5. Centroids of fission fragment masses as a function of center of mass scattering angle. Dashed lines indicate the position of $A_{CN}/2$. Typical error bars shown in the mass coordinate are statistical only. For systematic errors, see text.

from the difference of the reaction and inelastic cross sections, i.e.,

$$\sigma_{\text{capt}} = \frac{\pi}{k_\alpha^2} \sum_{l_\alpha} (2l_\alpha + 1) \left[1 - |S_l^{\alpha,\alpha}|^2 - \sum_\beta |S_l^{\alpha,\beta}|^2 \right] , \quad (2)$$

where β sums over all inelastic channels, and k_α and l_α are the entrance channel wave number and orbital angular momentum. This approach has been successful in reproducing measured fusion cross sections over a wide range of compound nuclei (from $A_{\text{CN}} \approx 50$ to $A_{\text{CN}} \approx 200$) with best results for the lighter systems. So far it has not been used to describe σ_{capt} for such heavy systems. Due to the truncated basis used in the coupled channels calculations, one still has to introduce an imaginary part into the optical potential. The authors of Ref. 23 have shown a method of constructing this imaginary potential while preserving the strong couplings to the direct reaction channels. They also show that in the limit of zero coupling the WKB results are obtained. Their method will be used here.

A. One-dimensional calculations

To determine, first, whether any enhancement exists in the capture cross section for $^{32}S + ^{238}U$, one-dimensional barrier penetration calculations were performed for the reaction cross section. For the real part of the nuclear potential the prescription of Akyüz and Winther[13] was used, while the imaginary part was taken to be a short range potential of Woods-Saxon squared form. The parameters used for the real potential are $V_0 = -74.7$ MeV, $a_0 = 0.68$ fm, and $r_0 = 1.18$ fm; for the volume imaginary part, $V_{0i} = -10$ MeV, $a_{0i} = 0.4$ fm, and $r_{0i} = 1.0$ fm. The Coulomb potential was calculated for a uniformly charged sphere with a radius equal to the sum of the target and projectile radii and a Coulomb radius parameter of 1.2 fm.

The transmission coefficients $T(l_\alpha)$ were then obtained by directly integrating the Schrödinger equation using the above "bare" nuclear potential. The validity of using such an imaginary potential has been examined in Ref. 23. The total capture cross section is calculated according to

$$\sigma_{\text{capt}}^{\text{bare}} = \frac{\pi}{k_\alpha^2} \sum_{l_\alpha} (2l_\alpha + 1) T(l_\alpha) .$$

Figure 6 shows the measured energy dependence of the capture cross section together with the predictions of this one-dimensional calculation (dashed line). Also plotted are the data points from Ref. 8 (open circles). Agreement between the two experiments, which used different experimental techniques, is very good. The figure also shows that while the cross section above the barrier is well reproduced within this simple one-dimensional model, there is substantial enhancement (> 100) in the experimental cross section at energies near and below the barrier.

B. The coupled channels method

Since the one-dimensional calculation underpredicts the cross section, we would like to determine whether the subbarrier enhancement in the capture cross section seen in Fig. 6 can be explained by including couplings to the very collective low lying excited states in ^{238}U. Barrier penetration through such a multi-dimensional potential energy surface has been calculated using the method of Ref. 23. For the system $^{32}S + ^{238}U$ these calculations were first performed by coupling just to the lowest 2^+ state in ^{238}U at 45 keV. Both nuclear and Coulomb excitation have been included and a value of $B(E2) = 12.3\ e^2b^2$ from Ref. 28 was used. The nuclear deformation parameter is calculated according to the scaling law of Ref. 29. The coupled channel equations were solved using the coupled channels versions of either of the codes PTOLEMY (Ref. 30) or ECIS (Ref. 31).

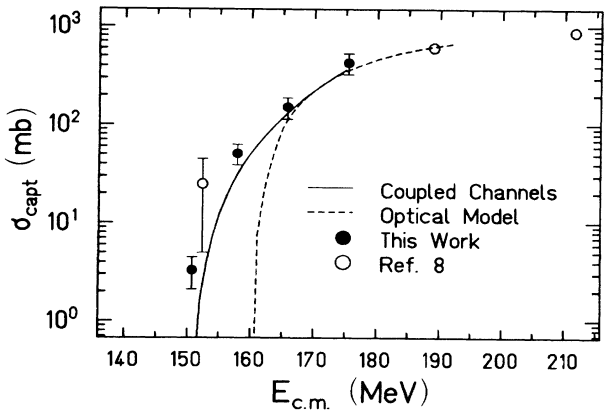

FIG. 6. The experimental capture excitation function compared to predictions of coupled channels and "bare" optical model calculations.

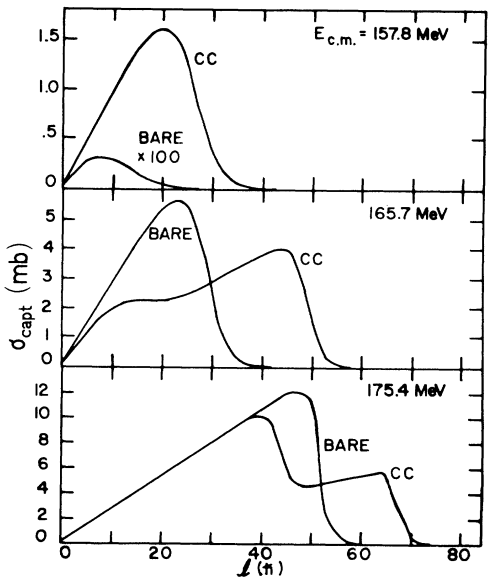

FIG. 7. Comparison of CC and "bare" spin distributions for $^{32}S + ^{238}U$ (see text).

The effect of coupling to the lowest 2^+ state in ^{238}U can be seen in Fig. 7, where the spin distributions, $\sigma_{\text{capt}}(l)=(2l+1)T_l$, calculated using coupled channels (CC) are compared to those using only the "bare" optical potential. The three highest energies are shown. The CC spin distributions (from ECIS) $\sigma_{\text{capt}}^{\text{CC}}(l)$ extend further in l space than the "bare" spin distributions $\sigma_{\text{capt}}^{\text{bare}}(l)$. An explanation of the shapes of $\sigma_{\text{capt}}^{\text{CC}}(l)$ has been given[32,33] by considering a simple two level system. Coupling between the two levels has the effect of splitting into two effective potentials the potential barrier seen in the entrance channel. One of these effective potentials is raised by the coupling and the other lowered. It is this splitting of the potential barrier that produces the structure seen in the spin distributions.

The results of using PTOLEMY or ECIS were virtually identical, except that ECIS allowed all partial waves up to $80\hbar$ to be included and the calculation converged for all these partial waves. Inclusion of higher partial waves was not possible due to the limited word size of the computer. The spin distributions shown in Fig. 7 indicate that including 80 partial waves is sufficient to describe the present reaction even at the highest energy.

Figure 6 also compares the capture excitation function as predicted by CC (solid curve) to the experimental data. The figure shows that the CC calculations predict significantly higher cross sections below the barrier than the "bare" optical model calculations (approximately 3 orders of magnitude at $E_{\text{c.m.}}=157.8$ MeV) and agree quite well with the data for energies near and above the barrier. Even the CC calculations still underpredict the data at the lowest energy. However, the agreement between the CC calculations and the data is much better here than in some other rotational systems where subbarrier fusion has been studied.[27] If the neck degrees of freedom are important in explaining the discrepancy between the calculations of Ref. 27 and the data discussed there, then a similar discrepancy would have been expected here. The relatively good agreement obtained here indicates the unimportance of such neck degrees of freedom for this reaction.

At $E_{\text{c.m.}}=150.7$ MeV the bombarding energy is below the minimum in the pocket of the potential described above. Hence the WKB and the "bare" optical model calculations yield zero cross section. In contrast, a capture cross section of 3.3 ± 1.2 mb is measured. The calculated cross section using CC predicts a value that is much less than the data, but still indicates a substantial lowering of the effective entrance channel potential and, hence, of the pocket.

C. Inclusion of higher lying states

The low lying states in ^{238}U are essentially rotational in character and therefore calculations including higher members in the rotational band may not appreciably change the calculated capture cross section since populating the 4^+ or higher levels proceeds at the expense of depopulating the 2^+ state. To test this hypothesis, calculations including higher lying states in ^{238}U were performed.

Because of the strong interplay between the Coulomb and nuclear excitation for $^{32}\text{S}+^{238}\text{U}$, calculations involving higher lying states in the target are difficult. With ECIS it is possible to include couplings up to the 6^+ at all energies. However, the number of partial waves that can be calculated become smaller as higher states are included and therefore the predicted cross sections become reliable only at lower energies: At $E_{\text{c.m.}}=157.8$ MeV a calculation using only 45 partial waves and coupling to the 2^+ state gives the same cross section as when 80 partial waves are included (see Fig. 7). Including the 4^+ state (and 45 partial waves) at $E_{\text{c.m.}}=157.8$ MeV leads to a predicted cross section equal to that for the 2^+ case (31.2 mb), confirming the above assumption.

V. FISSION FRAGMENT ANGULAR DISTRIBUTIONS

Recent measurements[3,12,34,35] of fragment angular distributions for similar reactions have yielded anisotropies that are much larger than those predicted by the rotating liquid drop model (RLDM). In this model one expects nearly isotropic angular distributions of the fission fragments due to the very compact saddle point configuration for such heavy systems.

This large discrepancy between measured angular distributions and the RLDM predictions is also expected for the present system, where the experimentally observed anisotropies are large (see Fig. 4), even at the lowest beam energy, since the predicted saddle point shape is very nearly spherical for the system $^{270}_{108}$X. In order to investigate this situation more quantitatively, we will compare, in this section, the measured data with predictions from an improved version of the standard transition state model, namely the flexible rotor model of Ref. 36 and, alternatively, with the results of a scission point transition state calculation closely following Ref. 6. Since the pertinent formalism has been developed elsewhere in the literature (Refs. 3–6, 10, 11, and 36), we will concentrate, in the following, only on the essential parameters of the different models.

A. Review of the formalism

In both saddle and scission point models the starting point for calculations of fission fragment angular distributions is (assuming zero channel spins)

$$W(\theta_{\text{c.m.}})\propto\sum_{I,K}\sigma(I)P_{\text{fiss}}(I,K,\theta_{\text{c.m.}})\ , \tag{3}$$

where the compound nucleus formation cross section $\sigma(I)$ should be identified with $\sigma_{\text{capt}}(l)$, and the fission probability P_{fiss} is obtained by assuming that at the relevant point of equilibration (saddle or scission) the system moves in the direction of the separation (or symmetry) axis. If K is the projection of I (or l) onto the symmetry axis, and $\rho(I,K)$ describes the level density at equilibrium, then

$$P_{\text{fiss}}(I,K,\theta_{\text{c.m.}})\propto\frac{2I+1}{2}\,|\,d^I_{0K}\,|^2\rho(I,K)\ . \tag{4}$$

It is only in the specification of $\rho(I,K)$ that the various models differ. Using a constant temperature approximation, $\rho(I,K)\propto\exp(-E_{\text{rot}}/T)$. E_{rot} is the rotational energy

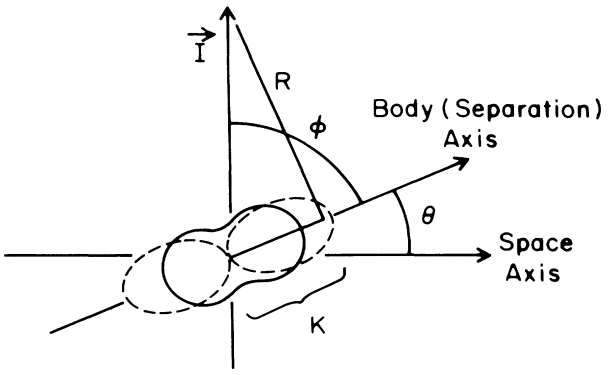

FIG. 8. Comparison between the saddle point (solid curve) and the scission point (dashed curve) transition shapes.

and T is the temperature at the transition state. The differences in the models are therefore essentially contained in the geometry used to describe the saddle or scission point configuration, and a pictorial representation of our approach is shown in Fig. 8.

In the saddle point approach the rotational energy $E_{\rm rot}$ is calculated assuming rigid rotation of a deformed spheroid, i.e.,

$$E_{\rm rot}=\frac{\hbar^2(I^2-K^2)}{2\mathscr{I}_\perp}+\frac{\hbar^2K^2}{2\mathscr{I}_{||}}\ , \tag{5}$$

where $\mathscr{I}_{\perp\,(||)}$ is the moment of inertia perpendicular (parallel) to the symmetry axis. The temperature at the saddle point is obtained from the excitation energy $E^*_{\rm sad}=E_{\rm CN}-E_{\rm def}-E_{\rm rot}$ using the usual Fermi gas formula $T\approx(E^*_{\rm sad}/a)^{1/2}$ with a level density parameter $a=A_{\rm CN}/8$. $E_{\rm CN}$ is the excitation energy of a spherical compound nucleus. In the flexible rotor model of Ref. 36 both the moments of inertia $\mathscr{I}$ and deformation energies $E_{\rm def}$ are calculated retaining their explicit dependence on K and this approach is used in the following.

In the scission point approach the excitation energy $E^*_{\rm scis}$ is similarly calculated as $E^*_{\rm scis}=E_{\rm CN}+Q_{\rm fiss}-E_{\rm int}-E_{\rm rot}$, where $Q_{\rm fiss}$ is the Q value for symmetric splitting of the compound nucleus and $E_{\rm int}$ is the interaction energy between the two touching equal mass spheroids (see Fig. 8). The temperature is again obtained from $T\approx(E^*_{\rm scis}/a)^{1/2}$ with $a=A_{\rm CN}/8$. The rotational energy is calculated using the touching spheroid approximation (Ref. 6). It is the elongation of the touching spheroids which influences the predicted anisotropy. Following Ref. 6, we choose axis ratios near 2:1.

B. Comparison of the model predictions to the results

The spin distributions, $\sigma(I)=\sigma_{\rm capt}(l)$, must be specified before the actual calculations can be performed. The most realistic spin distributions are those calculated by the CC approach as discussed in Sec. IV. A problem with those calculations is that, especially at the lowest energy, they do not match the experimental cross section. To investigate the influence on the anisotropies due to variations in the assumed spin distributions, we have also used the sharp cutoff approximation (SCO) and the optical model (OPT). For the optical model calculations the imaginary part of the nuclear potential was varied in such a way as to reproduce the measured cross sections (the real part is the same as in the CC calculations). This approach has the disadvantage of relying strongly on this *ad hoc* imaginary part and will yield roughly triangular spin distributions, which are at variance with what is presented in Fig. 7. Similarly, the sharp cutoff approximation is also of questionable validity, except at the highest energy, and is only included for completeness.

Figure 4 and Table II show that the experimental fission fragment anisotropy decreases very slowly with decreasing bombarding energy. Even at the lowest bombarding energies, anisotropies of the order of 2:1 are observed while, semiclassically, one would expect nearly isotropic angular distributions for fission following compound nucleus formation. To make this point more quantitative, we compare with the experimental data in Fig. 9 and Table II the predictions of a saddle point model, i.e.,

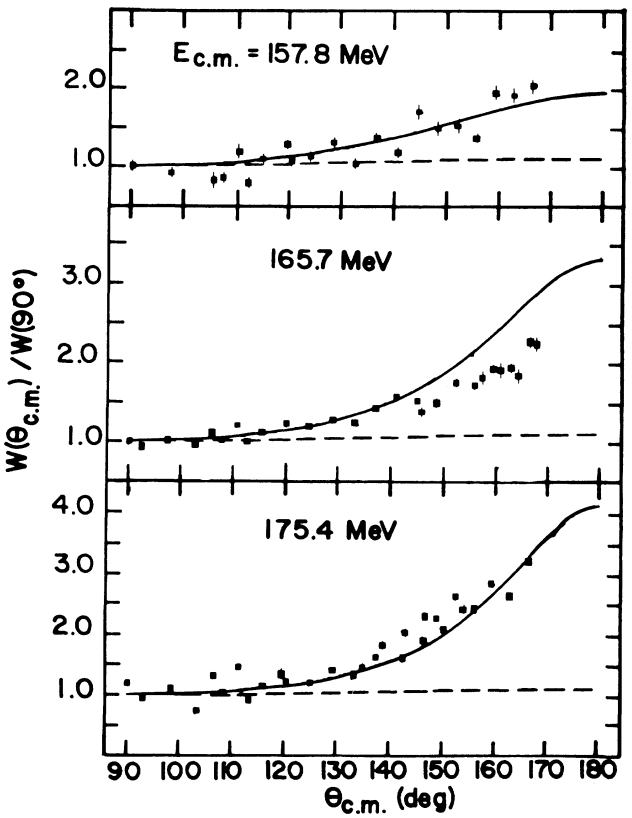

FIG. 9. Comparison of the predictions of the flexible rotor model (dashed curve) and the scission model (solid curve) of the text to the experimental data. In all calculations CC spin distributions were used.

TABLE II. Comparison of predictions of flexible rotor model of Ref. 36 and the scission point model for the system $^{32}S+^{238}U$. $Z^2/A=43.2$ and $E_{bar}=161.8$ MeV.

$E_{c.m.}$ (MeV)	T^{sad} (MeV)	T^{scis} (MeV)	Spin distrib.	l_{rms} ($\hbar$)	σ_{capt}^{calc} (mb)	$W(164°)/W(90°)$ Saddle	Scission	Expt.
150.7	1.14	1.59	CC	30.1	0.03	1.10	2.43	
			OPT	35.2	4.3	1.13	2.76	See text
			SCO	3.8	3.0	1.00	1.03	
157.8	1.22	1.63	CC	19.0	31.2	1.11	1.80	
			OPT	15.2	48.1	1.09	1.54	2.05±0.43
			SCO	12.3	47.8	1.07	1.37	
165.7	1.30	1.70	CC	33.0	130.1	1.12	2.68	
			OPT	26.4	141.0	1.10	2.19	2.10±0.37
			SCO	22.2	144.0	1.12	2.05	
175.4	1.37	1.78	CC	40.9	375.4	1.11	3.03	
			OPT	39.7	404.6	1.12	3.08	2.94±0.62
			SCO	39.2	416.5	1.12	3.08	

the flexible rotor model (shown as the dashed curve), and the scission point model (the solid curve) described above with the experimental data. In Fig. 9 the calculations are shown only for the case of CC spin distributions. Shown in the table are the experimental anisotropies of the angular distributions and the calculations using the three different spin distributions: SCO and OPT distributions fitted to σ_{capt}^{expt} and the CC spin distributions. Also shown is the predicted cross section $\sigma_{capt}=\sum_l(2l+1)T_l$ and l_{rms} for each distribution.

Because the fission barrier is so small for the system $^{32}S+^{238}U$ ($\approx$300 keV), the saddle point shape is nearly spherical, and hence the angular distributions predicted by the flexible rotor model are nearly isotropic. This system has a fission barrier $B_{fiss}(l=0)\ll T^{sad}$ and thus the discrepancy between the data and these predictions is not unexpected. In contrast, the scission point shape is much more elongated and therefore substantial anisotropies are predicted. Also shown in the table is that as l_{rms} increases, the anisotropy predicted by either model increases.

At $E_{c.m.}=150.7$ MeV (not shown in Fig. 9) the CC calculation yielded a cross section that was much smaller than the measured one. Using this spin distribution, the scission model predicts a value of $W(164°)/W(90°)=2.43$. Based on the same extrapolation used to calculate the integrated cross section, the experimental value for the anisotropy of the angular distribution is estimated to be 1.90 ± 0.6. The quoted error is due to experimental errors and the extrapolated value of $W(90°)$.

At the next higher energy, $E_{c.m.}=157.8$ MeV, the anisotropy predicted by the scission model based on CC and OPT spin distributions is less than the experimental value, but within the uncertainty. The sensitivity of the angular distribution to the shape of the spin distribution is again evident, since even though the total capture cross section is underpredicted by about 50% ($\sigma_{capt}^{expt}=51\pm12$ mb) by the CC calculations, the predicted anisotropy follows the trend in the data quite well (see Fig. 9). The l_{rms} values for the CC and OPT spin distributions are larger than the SCO value and, hence, using the latter spin distribution, the experimental data are underpredicted.

Above the barrier at $E_{c.m.}=165.7$ and 175.4 MeV the predictions based on all three spin distributions are clustered around the data (see Fig. 9). This is expected since Table II shows that the l_{rms} values for all spin distributions are very close. The CC predictions are slightly above the data at the lower of the two energies and this is explained in terms of its larger value of l_{rms}.

Based on the calculations presented here, it is concluded that the saddle point transition state theory does not work for the system $^{32}S+^{238}U$. However, the scission point model described above reproduces the measured anisotropies of the fission fragment angular distributions at these energies when realistic spin distributions (i.e., CC) are used.

VI. CONCLUSIONS

Capture cross sections for $^{32}S+^{238}U$ have been studied at energies near and below the *s*-wave interaction barrier. The measured fission fragment angular distributions together with the mass versus angle correlations indicate the presence of nonequilibrium reaction processes in agreement with previous findings.[8,15,17] Despite the presence of these processes, the excitation function can be successfully describing using the coupled channels formalism. This result is not surprising since the coupled channels method is only based on unitarity as long as those reaction channels that are strongly coupled to the elastic channel are included. Assuming that the most important channels in this system are due to inelastic and capture processes, and using the nuclear potential of Ref. 13, this leads to good agreement between the calculations and the data, except at the lowest energy. In these calculations it is, in fact, sufficient to only include the lowest lying 2^+ state in ^{238}U. Inclusion of higher lying states in the target has very little effect on the calculated cross section. This is plausible since in ^{238}U, which is a collective rotor, all the

inelastic flux passes through the first 2^+ state, which is strongly coupled to the ground state. One should note that for the system studied here the effective fissility is close the predicted onset of the extra push mechanism. The present data do not indicate the need for this mechanism, justifying *a posteriori* the neglect of extra push in the present calculation.

The failure of the saddle point model to reproduce the measured angular distributions is in agreement with the observed nonequilibrium aspects of this reaction. On the basis of the angular distributions alone, one cannot rule out that the reaction proceeds through a compound nucleus with equilibration at the scission configuration. At energies above the interaction barrier and for lighter systems, Back[3,34] concludes that the saddle point model is more appropriate. Either approach cannot explain the mass-angle correlations observed here and in Refs. 8, 15, and 17. Our data and analysis are then consistent with the interpretation that the dominant reaction mechanism is capture and reseparation of fragments rather than true compound nucleus formation followed by fission.

ACKNOWLEDGMENTS

The authors acknowledge useful and stimulating discussions with Dr. M. Prakash, Dr. N. Alamanos, Dr. M. J. Rhoades-Brown, and Dr. J. M. Alexander. Also acknowledged is the help provided by Dr. Ludger Ricken and Dr. Zhang Pei-Hua in the initial phases of the experiments. This work was supported in part by the National Science Foundation.

*Present address: Gesellschaft für Schwerionenforschung mbH, Postfach-110541, 6100 Darmstadt 11, Federal Republic of Germany.

†Present address: Department of Physics, Hope College, Holland, MI 49423.

[1]L. C. Vaz, J. M. Alexander, and G. R. Satchler, Phys. Rep. **69**, 373 (1981), and references therein.

[2]R. G. Stokstad, W. Reisdorf, K. D. Hildenbrand, J. V. Kratz, G. Wirth, R. Lucas, and J. Poitou, Z. Phys. A **295**, 269 (1980).

[3]B. B. Back, Phys. Rev. C **31**, 2104 (1985), and references therein.

[4]P. D. Bond, Phys. Rev. Lett. **52**, 414 (1984); Phys. Rev. C **32**, 471 (1985); **32**, 483 (1985).

[5]H. H. Rossner, J. R. Huizenga, and W. U. Schröder, Phys. Rev. Lett. **53**, 38 (1984); H. H. Rossner, J. R. Huizenga, and W. U. Schröder, Phys. Rev. C **33**, 560 (1986).

[6]R. Freifelder, M. Prakash, and J. M. Alexander, Phys. Rep. **133**, 315 (1986).

[7]W. J. Swiatecki, Nucl. Phys. **A376**, 275 (1982); S. Bjørnholm, *ibid.* **A387**, 51 (1982).

[8]W. Q. Shen, J. Albinski, R. Bock, A. Gobbi, S. Gralla, K. D. Hildenbrand, N. Herrmann, J. Kuzminski, W. F. J. Müller, H. Stelzer, J. Töke, B. B. Back, S. Bjørnholm, S. P. Sørensen, A. Olmi, and G. Guarino, Europhys. Lett. **1**, 113 (1986); W. Q. Shen, in *Proceedings of the XXIIIrd International Winter Meeting on Nuclear Physics,* Bormio, Italy, 1985, edited by I. Iori (Ricerca Scientifica ed Educazione Permanente, Milano, 1985), Vol. 47, p. 669.

[9]L. C. Vaz and J. M. Alexander, Phys. Rep. **97**, 1 (1983).

[10]A. Bohr, in Proceedings of the United Nations International Conference on the Peaceful Uses of Atomic Energy, United Nations, New York, 1956, Vol. 2, p. 115; I. Halpern and V. M. Strutinski, in Proceedings of the United Nations International Conference on the Peaceful Uses of Atomic Energy, United Nations, Geneva, 1958, Vol. 15, p. 408; and T. Ericson and V. Strutinski, Nucl. Phys. **8**, 284 (1958).

[11]J. A. Wheeler, in *Fast Neutron Physics, Part II,* edited by J. B. Marion and J. L. Fowler (Wiley, New York, 1963), p. 2051.

[12]K. T. Lesko, S. Gil, A. Lazzarini, V. Metag, A. G. Seamster, and R. Vandenbosch, Phys. Rev. C **27**, 2999 (1983); R. Vandenbosch, T. Murakami, C.-C. Sahm, D. D. Leach, A. Ray, and M. J. Murphy, Phys. Rev. Lett. **56**, 1234 (1986).

[13]R. Ö. Akyüz and A. Winther, in *Nuclear Structure and Heavy Ion Reactions, Proceedings of the Enrico Fermi International School of Physics (1979),* edited by R. A. Broglia, R. A. Ricci, and C. H. Dasso (North-Holland, Amsterdam, 1981).

[14]V. E. Viola, Jr., Nucl. Data **1**, 391 (1965).

[15]J. Töke, R. Bock, G. X. Dai, A. Gobbi, S. Gralla, K. D. Hildenbrand, J. Kuźminski, W. F. J. Müller, A. Olmi, H. Stelzer, B. B. Back, and S. Bjørnholm, Nucl. Phys. **A440**, 327 (1985); W. Q. Shen, J. Albinski, A. Gobbi, S. Gralla, K. D. Hildenbrand, N. Herrmann, J. Kuzminski, W. F. J. Müller, H. Stelzer, J. Töke, B. B. Back, S. Bjørnholm, and S. P. Sørenson, submitted to Phys. Rev. C.

[16]U. Lynen, H. Stelzer, A. Gobbi, H. Sann, and A. Olmi, Nucl. Instrum. Methods **162**, 657 (1979).

[17]R. Bock, Y. T. Chu, M. Dakowski, A. Gobbi, E. Grosse, A. Olmi, H. Sann, D. Schwalm. U. Lynen, W. Müller, S. Bjørnholm, H. Esbensen, W. Wölfli, and E. Morenzoni, Nucl. Phys. **A388**, 334 (1982).

[18]M. Rajagopalan, D. Logan, J. W. Ball, M. Kaplan, H. Delagrange, M. F. Rivet, J. M. Alexander, L. C. Vaz, and M. S. Zisman, Phys. Rev. C **25**, 2417 (1982).

[19]W. Reisdorf, F. P. Hessberger, K. D. Hildenbrand, S. Hofmann, G. Münzenberg, K.-H. Schmidt, J. H. R. Schneider, W. F. W. Schneider, K. Sümmerer, G. Wirth, J. V. Kratz, and K. Schlitt, Phys. Rev. Lett. **49**, 1811 (1982).

[20]G. M. Berkowitz, P. Braun-Munzinger, J. S. Karp, R. H. Freifelder, T. R. Renner, and H. W. Wilschut, Phys. Rev. C **28**, 667 (1983).

[21]H. J. Krappe, in *Proceedings of the Symposium on Deep-Inelastic and Fusion Reactions With Heavy-Ions, Berlin, 1979,* Vol. 117 of *Lecture Notes in Physics,* edited by W. von Oertzen (Springer, New York, 1980), p. 312.

[22]H. J. Krappe, J. R. Nix, and A. J. Sierk, Phys. Rev. C **20**, 992 (1979).

[23]M. J. Rhoades-Brown and P. Braun-Munzinger, Phys. Lett. **136B**, 19 (1984).

[24]M. J. Rhoades-Brown and M. Prakash, Phys. Rev. Lett. **53**, 333 (1984).

[25]S. C. Pieper, M. J. Rhoades-Brown, and S. Landowne, Phys. Lett. **162B**, 43 (1985).

[26]D. M. de Castro Rizzo and N. Alamanos, Nucl. Phys. **A443**, 525 (1985).

[27]M. J. Rhoades-Brown, P. Braun-Munzinger, M. Prakash, and S. Sen, in *Proceedings of the International Conference on Fusion Reactions Below the Coulomb Barrier,* Cambridge, Mass., edited by S. G. Steadman (Springer, New York, 1985), p. 162.

[28]E. N. Shurshikov, M. F. Filchenkov, Yu. F. Jaborov, and A. I. Khovanovich, Nucl. Data Sheets **38**, 277 (1983).
[29]D. L. Hendrie, Phys. Rev. Lett. **31**, 478 (1973).
[30]M. Rhoades-Brown, M. H. Macfarlane, and S. C. Pieper, Phys. Rev. C **21**, 2417 (1980); **21**, 2436 (1980).
[31]J. Raynal, Phys. Rev. C **23**, 2571 (1981); CEN-Saclay Report DPh-t/7148, 1971.
[32]C. H. Dasso, in *Proceedings of the XXIInd International Winter Meeting on Nuclear Physics,* Bormio, Italy, 1984, edited by I. Iori (Ricerca Scientifica ed Educazione Permanente, Milano, 1984), Vol. 35, p. 716.
[33]See Ref. 27, p. 182.
[34]B. B. Back, H.-G. Clerc, R. R. Betts, B. G. Glagola, and B. D. Wilkins, Phys. Rev. Lett. **46**, 1068 (1981); B. B. Back, R. R. Betts, J. E. Gindler, B. D. Wilkins, S. Saini, M. B. Tsang, C. K. Gelbke, W. G. Lynch, M. A. McMahan, and P. A. Baisden, Phys. Rev. C **32**, 195 (1985).
[35]M. B. Tsang, H. Utsunomiya, C. K. Gelbke, W. G. Lynch, B. B. Back, S. Saini, P. A. Baisden, and M. A. McMahan, Phys. Lett. **129B**, 18 (1983).
[36]M. Prakash, V. S. Ramamurthy, S. S. Kapoor, and J. M. Alexander, Phys. Rev. Lett. **52**, 990 (1984).